

A SPECTACULAR MOLECULAR OUTFLOW IN THE MONOCEROS OB1 MOLECULAR CLOUD

MICHAEL MARGULIS,^{1,2} CHARLES J. LADA,² TETSUO HASEGAWA,³ SAEKO S. HAYASHI,³ MASHIKO HAYASHI,³
 NORIO KAIFU,³ IAN GATLEY,⁴ THOMAS P. GREENE,² AND ERICK T. YOUNG²

Received 1989 April 11; accepted 1989 September 28

ABSTRACT

We present detailed observations of CO, CS, infrared continuum, and H₂ emission from a large, highly collimated, bipolar outflow in the Monoceros OB1 molecular cloud. From the high-resolution observations of CO emission, we find evidence that molecular gas in the outflow is contained in a shell with higher velocity material situated interior to lower velocity material. We also find the observed velocities of outflow emission to increase with increasing distance from the center of the outflow, and the gas in the outflow to be clumpy. A peak in the distribution of CS emission from the ambient cloud has also been found between the two outflow lobes and may indicate the existence of a dense core of gas in which the driving source of the outflow has formed. In addition, we have detected shock-excited molecular hydrogen emission from the blueshifted lobe of the outflow.

Six 2 μm sources have been detected in the direction of the outflow. Of these, two are the most likely candidate driving sources. One source is situated coincident on the sky with the peak of the CS emission, and the other has a spectral energy distribution which is steeply rising toward the far-infrared. However, analysis of the near-infrared and *IRAS* observations suggests that any driving source for the outflow must have a bolometric luminosity less than about 4.5 L_⊙. The ratio of driving source radiant luminosity to flow mechanical luminosity is less than or equal to 1.8, an order of magnitude lower than that determined for any other known outflow source. This suggests that it is unlikely for this flow to be driven by stellar radiation from a central source since conversion efficiencies in excess of 50% from stellar luminosity to flow mechanical luminosity would be required.

Subject headings: infrared: sources — interstellar: molecules — nebulae: individual (Mon OB1) — nebulae: internal motions

I. INTRODUCTION

Knowledge of the detailed structure of molecular outflows is important for our understanding of star formation. To date, however, the structure of few molecular outflows has been studied in great detail. The best studied outflow is the nearby, highly collimated outflow in the dark cloud L1551 (Snell, Loren, and Plambeck 1980; Snell and Schloerb 1985; Uchida *et al.* 1986; Moriarty-Schieven *et al.* 1987; Moriarty-Schieven and Snell 1988). Evidence has been found that much of the molecular material in this outflow is confined to a relatively thin shell, that material appears to be accelerating in the outflow, and that some material in the outflow is situated in clumps. It would be useful to investigate the structure of other nearby, highly collimated outflows, in order to test whether these characteristics of the outflow in L1551 are common to outflows in general.

During the course of a survey of the Monoceros OB1 molecular cloud for high-velocity emission, Margulis and Lada (1986) identified an outflow with striking, highly collimated, bipolar morphology (outflow NGC 2264G; Margulis, Lada, and Snell 1988). This spectacular outflow is very energetic for its mass, possessing some very high velocity outflow emission (outflow material has been observed from -35 km s^{-1} to 54

km s^{-1}). However, in spite of its spectacular appearance and relatively large luminosity, there is no strong *IRAS* source associated with it. Because of its striking morphology and high velocities, detailed observations of this outflow are likely to place severe constraints on models of molecular outflows in general. In this paper we present such observations and discuss both the detailed structure and energetics of this spectacular object.

II. OBSERVATIONS

In order to obtain as complete a picture as possible of the morphology and energetics of the outflow (hereafter outflow G), observations of the flow and the surrounding region were made using a number of spectral lines and continuum emission in a number of infrared bands as probes. Observations of emission from the $J = 1-0$ and $J = 2-1$ transitions of CO were made in order to probe the structure and energetics of outflow G itself, observations of $J = 2-1$ emission from CS were made in order to investigate the structure of the molecular cloud surrounding the outflow, observations of continuum emission in eight bands from 1 to 100 μm were made in order to search for a young stellar object associated with outflow G, and observations of 2 μm spectral line emission from molecular hydrogen were made in order to search for shock-excited gas. The details of these observations are discussed below.

Using the Nobeyama Radio Observatory 45 m telescope⁵ during February and March of 1986, we have made a complete

¹ Five College Radio Astronomy Observatory and Department of Physics and Astronomy, University of Massachusetts.

² Steward Observatory, University of Arizona.

³ Nobeyama Radio Observatory and Department of Astronomy, University of Tokyo.

⁴ National Optical Astronomy Observatories.

⁵ NRO, a branch of the Tokyo Astronomical Observatory, is a facility open for the general use by researchers in the field of astronomy and astrophysics.

map of emission from the $J = 1-0$ transition of CO toward outflow G. The region mapped (shown in Figs. 1, 2, and 3) was sampled every $15''$ with a beam $14''$ in width. Altogether 297 positions were observed. These observations were made with a spectral resolution of 250 KHz or 0.65 km s^{-1} . The resulting data are presented here with velocities given with respect to the local standard of rest and temperatures expressed on the T_R^* scale (Kutner and Ulich 1981) as measured on the NRAO 11 m telescope. In order to express the temperatures on this scale, raw temperatures measured at NRO were scaled up by a factor of 3.2 and then by an additional factor of 0.87. The factor of 3.2 is that suggested in Lada *et al.* (1988) for a CO emission source larger than the NRO beam. It was arrived at by comparing a spectrum of CO $J = 1-0$ emission from Orion A taken on the NRAO 11 m telescope with a convolution of spectra taken at NRO toward the same source. The convolution of NRO spectra was made in order to compare NRO and NRAO spectra of Orion A as if both were made with the same beam size ($66''$). Details of this calibration procedure are given in Lada *et al.* The additional factor of 0.87 was used in order to correct for the fact that the NRO dish was resurfaced between the time these observations of outflow G and the observations of Orion A for calibration were made. This factor is just equal to the ratio of the raw peak temperatures seen in individual spectra of Orion A made at NRO before and after resurfacing. In general, while this calibration procedure is somewhat indirect, we do not expect errors in the absolute calibration of the

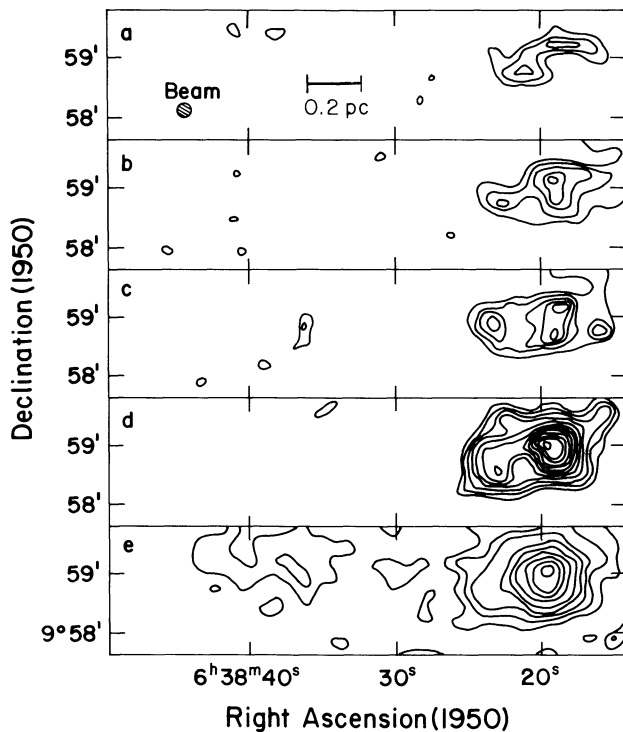


FIG. 1.—Maps of integrated intensity of CO $J = 1-0$ emission from outflow G. The velocity intervals over which the integrated intensities used to make the maps were calculated are -12 to -9 km s^{-1} for map (a), -9 to -6 km s^{-1} for map (b), -6 to -3 km s^{-1} for map (c), -3 to 0 km s^{-1} for map (d), and 0 to 3 km s^{-1} for map (e). In maps (a) through (d) the lowest contour is at 0.6 K km s^{-1} and the contour levels increase in steps of 0.2 K km s^{-1} . In map (e) the lowest contour level is at 1.5 K km s^{-1} , and the contour levels increase in steps of 0.5 K km s^{-1} . A 0.2 pc fiducial marker is shown in Fig. 1a.

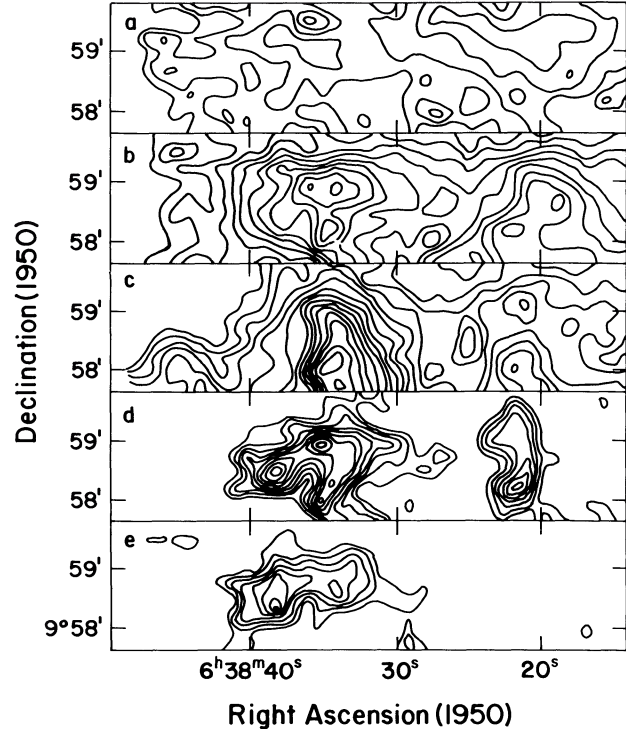


FIG. 2.—Maps of integrated intensity of CO $J = 1-0$ emission from outflow G. The velocity intervals over which the integrated intensities used to make the maps were calculated are 3 to 6 km s^{-1} for map (a), 6 to 9 km s^{-1} for map (b), 9 to 12 km s^{-1} for map (c), 12 to 15 km s^{-1} for map (d), and 15 to 18 km s^{-1} for map (e). The lowest contour levels in maps (a) through (e) are 5.0 , 3.0 , 2.0 , 1.0 , and 0.6 K km s^{-1} , respectively, and the contour levels increase in steps of 0.5 , 0.5 , 0.5 , 0.2 , and 0.2 K km s^{-1} . The lowest contour levels in maps (a) through (c) are on the eastern ends of the maps. The prominent features in maps (a) through (c) at about $6^{\text{h}}38^{\text{m}}22^{\text{s}}$, and in maps (b) and (c) at about $6^{\text{h}}38^{\text{m}}34^{\text{s}}$ are peaks.

CO data in this paper to be greater than 25%. On the T_R^* scale resulting from this method the peak temperature of Orion A in an individual spectrum taken with the 45 m telescope is 86 K. The 1σ rms noise in a typical spectrum is 0.7 K.

Using the NRAO 12 m telescope⁶ during February of 1987 observations of $J = 2-1$ emission from CO in outflow G were also made. These observations were made in a strip along the center of the outflow at $\delta_{1950} = 9^{\circ}58'42''$. Individual observations along the strip were spaced by $30''$. The resolution achieved in these observations was $33''$. The resulting data are presented here with velocities expressed with respect to the local standard of rest and temperatures expressed as T_R^* . The temperature scale was calibrated using the chopper wheel method as outlined in Ulich and Haas (1976) and Kutner and Ulich (1981). We expect that errors in the absolute temperatures obtained in this manner are not greater than 10%. On this scale the peak temperature of Orion A is 69 K. The 1σ rms noise achieved at a typical position in the strip is about 0.14 K .

Using the FCRAO 14 m telescope⁷ during March and May of 1988 observations of $J = 2-1$ emission from CS associated

⁶ The National Radio Astronomy Observatory is operated by Associated Universities Inc., under contract with the National Science Foundation.

⁷ The Five College Radio Astronomy Observatory is operated with support from the National Science Foundation under grant AST 88-15406 and with permission of the Metropolitan District Commission of the Commonwealth of Massachusetts.

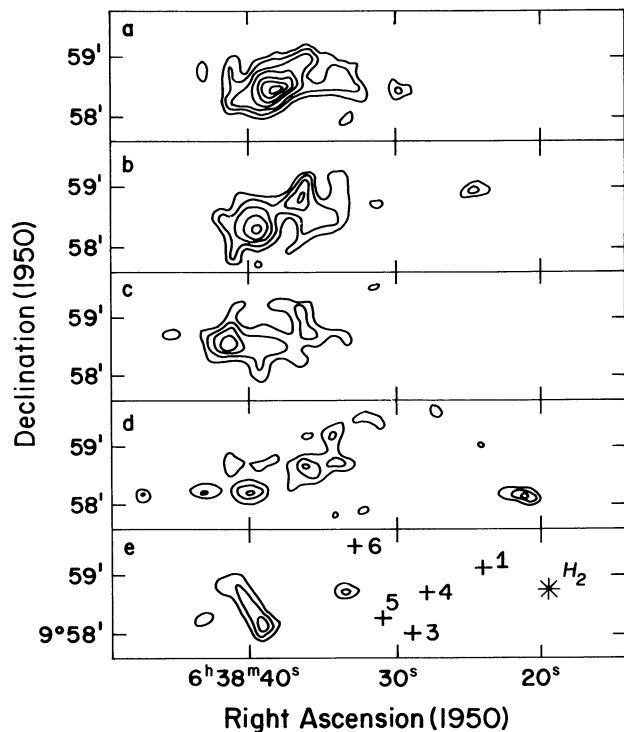


FIG. 3.—Maps of integrated intensity of CO $J = 1-0$ emission from outflow G. The velocity intervals over which the integrated intensities used to make the maps were calculated are 18 to 21 km s^{-1} for map (a), 21 to 24 km s^{-1} for map (b), 24 to 27 km s^{-1} for map (c), 27 to 30 km s^{-1} for map (d), and 30 to 33 km s^{-1} for map (e). The lowest contour levels in the maps are at 0.6 K km s^{-1} . The contour levels in the maps increase in steps of 0.2 K km s^{-1} . Positions of the near-infrared sources identified in this region are marked with plus signs (labeled by IRS number) in Fig. 3e. Source IRS 2 lies outside the boundary of the figure. The position where molecular hydrogen emission was detected is also marked with an asterisk. The sizes of the symbols denote positional uncertainties for the sources.

with outflow G were also made. These observations were made with a resolution of $52''$ and with $45''$ spacing throughout the region shown in Figure 4. The temperature scale was calibrated using the chopper wheel method as outlined in Ulich and Haas (1976) and is expressed as T_R^* (Kutner and Ulich 1981). We expect that errors in the absolute temperatures obtained in this manner are not greater than 10%. The 1σ rms noise achieved at positions east of $\alpha_{1950} = 6^{\text{h}}38^{\text{m}}28^{\text{s}}$ was about 0.12 K, while the 1σ noise achieved at positions west of $\alpha_{1950} = 6^{\text{h}}38^{\text{m}}28^{\text{s}}$ was about 0.07 K.

Observations of near-infrared emission in the J (1.2 μm), H (1.6 μm), K (2.2 μm), and L' (3.8 μm) bands from outflow G were also made. These observations were made using an InSb detector cooled to solid nitrogen temperature on the United Kingdom Infrared Telescope (UKIRT) on Mauna Kea, Hawaii, during January of 1986, and using Steward Observatory's 2 μm camera mounted on the University of Arizona's 61 inch (1.5 m) telescope on Mount Bigelow, Arizona, during April of 1988. Searches for near-infrared point sources toward outflow G were made in the H , K , and L' bands. The 3σ detection limits of the searches made at UKIRT were 14.9 magnitudes at K and 10.5 magnitudes at L' . The regions searched (a rectangle $28'' \times 2'$ centered at $\alpha_{1950} = 6^{\text{h}}38^{\text{m}}31^{\text{s}}.1$, $\delta_{1950} = 9^{\circ}58'42''$ at K and a rectangle $18'' \times 1'$ centered at $\alpha_{1950} = 6^{\text{h}}38^{\text{m}}29^{\text{s}}.4$, $\delta_{1950} = 9^{\circ}58'26''$ at L') using UKIRT were sampled every $19''$ with a $19''.6$ aperture at K and every $8''$ with

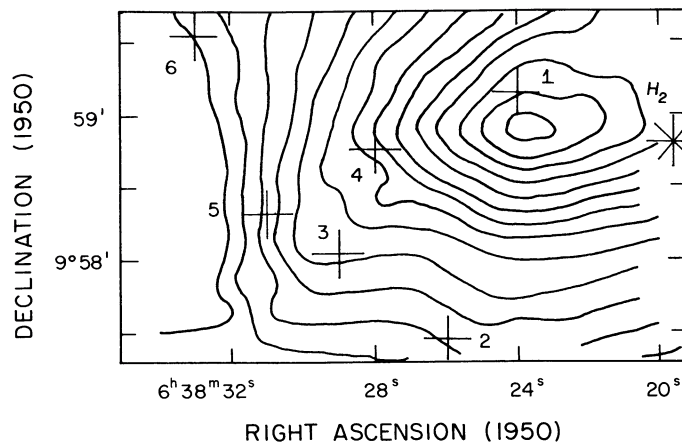


FIG. 4.—Map of the integrated intensity of emission from the $J = 2-1$ transition of CS in outflow G. The velocity interval over which the integrated intensities used to make the map were calculated was 3.5 km s^{-1} to 6.0 km s^{-1} . The contour levels start at 0.10 K km s^{-1} on the left and increase in steps of 0.05 K km s^{-1} to the right. The 1σ noise in the map is about 0.10 K km s^{-1} east of $\alpha_{1950} = 6^{\text{h}}38^{\text{m}}28^{\text{s}}$ and 0.06 K km s^{-1} west of $\alpha_{1950} = 6^{\text{h}}38^{\text{m}}28^{\text{s}}$. Positions of the near-infrared sources identified in the region are marked with plus signs (labeled by IRS number), and the position where molecular hydrogen emission was detected is marked with an asterisk. The sizes of the symbols denote positional uncertainties for the sources.

a $12''.4$ aperture at L' . The 3σ detection limits of the searches made at the 1.5 m telescope were 15.7 magnitudes at H and 14.2 magnitudes at K . The region searched was a box $8''.2 \times 2''.6$ centered at $\alpha_{1950} = 6^{\text{h}}38^{\text{m}}25^{\text{s}}.1$, $\delta_{1950} = 9^{\circ}58'28''$. The resolution of these observations was $3''$ and the sample spacing was $1''.2$. Photometry at H and K and in some cases at J and L' was obtained for the point sources identified which might possibly be associated with outflow G.

A search for $v = 1-0 S(1)$ emission from molecular hydrogen in outflow G was also made using the UKIRT facility. The region searched (the same as that searched at K using the UKIRT facility) was sampled every $19''$ with a $19''.6$ aperture. At the one position where H_2 emission was detected a spectrum of the 2 μm emission was taken using a circular variable filter and the InSb detector. The spectrum was made with a spectral resolution of 0.85% and an aperture $19''.6$ in width.

Finally, co-added maps made from IRAS⁸ survey (see Margulis and Lada 1986 and Margulis, Lada, and Young 1989) were carefully inspected to search for the presence of cold infrared point sources associated with outflow G. The 3σ detection limits of these searches were 0.1, 0.2, 0.3, and 2.6 Jy at 12, 25, 60, and 100 μm respectively.

III. RESULTS

a) Morphology of the Molecular Outflow

Presented in Figures 1 through 3 is a sequence of maps made at NRO of the integrated intensity of $J = 1-0$ emission from CO in outflow G. The integrated intensities in the maps were calculated over 3 km s^{-1} intervals starting with the bluest outflow emission (-12 km s^{-1} to -9 km s^{-1}) in Figure 1a and ending with the reddest outflow emission (30 km s^{-1} to 33 km s^{-1}) in Figure 3e. Also presented in Figures 5 and 6 are

⁸ The Infrared Astronomical Satellite was developed and operated by the Netherlands Agency for Aerospace Programs (NIVR), the US National Aeronautics and Space Administration (NASA), and the UK Science and Engineering Research Council (SERC).

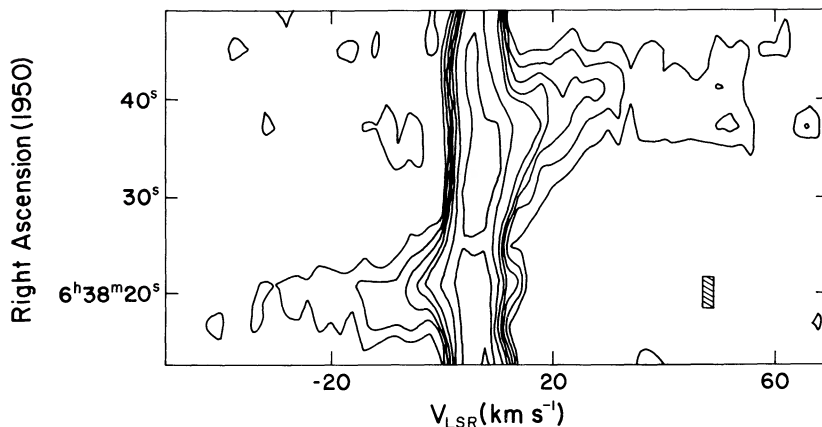


FIG. 5.—Position-velocity map of CO $J = 1-0$ emission from outflow G along $\delta_{1950} = 9^{\circ}58'28''$. Contour levels are at 0.2, 0.4, 0.6, 0.8, 1.0, 2.0, and 4.0 K. The hatch-marked rectangle denotes the resolution of the map.

position-velocity maps of CO $J = 1-0$ and $J = 2-1$ emission, respectively, made from spectra taken along the long axis ($\delta_{1950} = 9^{\circ}58'28''$ for Fig. 5 and $9^{\circ}58'42''$ for Fig. 6) of outflow G. The position-velocity map of $J = 1-0$ emission was made from the data base presented in Margulis, Lada, and Snell (1988) using the FCRAO 14 m telescope, while the map of $J = 2-1$ emission was made from data obtained using the NRAO 12 m telescope as described in § II. The observations from which these two maps were made were spaced by $60''$ and $30''$ respectively along the outflow's axis. As can be seen, both the integrated intensity and position-velocity maps contain a plethora of information pertaining to the velocity and spatial structure of the outflow. It is the purpose of this section to point out the salient morphological features contained in these maps.

It is especially clear from the position-velocity maps that the highest velocity emission (measured from line center) observed toward outflow G is at the far ends of the outflow lobes. This is perhaps most obvious in the case of the red wing emission in Figure 5, but it can also be seen in the case of the blue lobe and in the $J = 2-1$ map in Figure 6. A comparison of the integrated intensity maps in Figures 1 to 3 also shows this morphology,

with emission at the greatest velocities from line center lying farthest from the center of the map. It is also clear from the maps that emission at each velocity moves outward from the outflow center with increasing velocity. Once again this is most clear in the case of the red wing emission in Figures 5 and 6 in which one can follow the peak of the ridge of wing emission outwards from low to high velocity. However, this behavior can also be seen in the nearly unresolved blue lobe in the $J = 2-1$ map and in the integrated intensity maps presented in Figures 1–3. A comparison of the integrated intensity maps at low and high velocities in each lobe shows that higher velocity emission is confined to regions both smaller and farther out from the outflow center than lower velocity emission. In order to illustrate this point further, a graph quantitatively showing the progression of the outflow lobes away from the center of the outflow is displayed in Figure 7. In this graph the variation of the “average” distance of each lobe from the outflow's center is plotted as a function of velocity. The “average” distances were calculated from the positions of the outflow lobes in Figures 1 through 3. They are just the averages of the nearest and farthest distances (in right ascension and measured at the 1.0 ± 0.4 K km s^{-1} level) that the lobes get from the

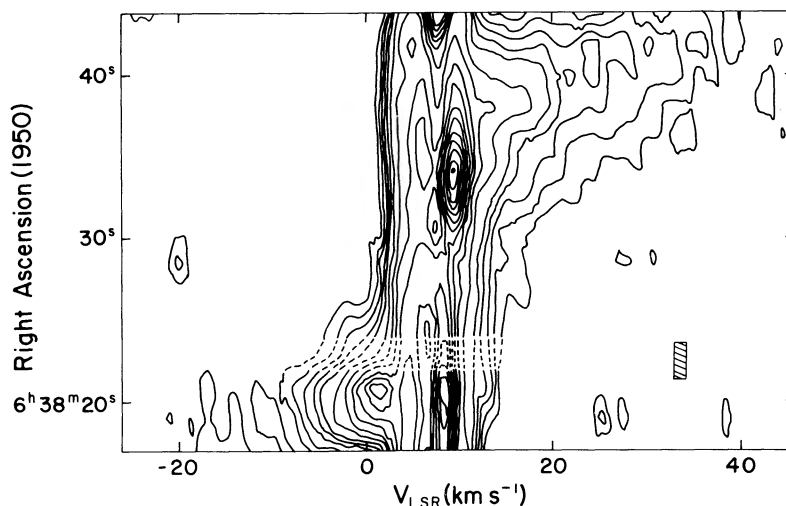


FIG. 6.—Position-velocity map of CO $J = 2-1$ emission from outflow G along $\delta_{1950} = 9^{\circ}58'42''$. Contour levels are at 0.2, 0.4, 0.6, 0.8, 1.0, 1.5, 2.5, 3.0, 3.5, 4.0, 4.5, 5.0, 5.5, 6.0, and 6.5 K. No data were taken at the right ascension of the dashed contours. The hatch-marked rectangle denotes the resolution of the map.

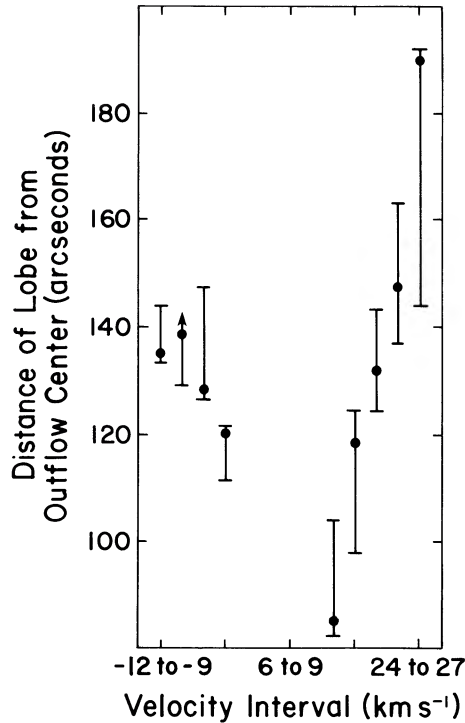


FIG. 7.—Graph showing the variation of the average distance of each outflow lobe from the outflow's center as a function of velocity. Note that material moving at higher velocities from ambient ($\approx 5 \text{ km s}^{-1}$) is situated farther from the outflow center than material moving at lower velocities.

center of the outflow in each velocity interval. The center of the outflow was taken to be at $\alpha_{1950} = 6^{\text{h}}41^{\text{m}}48^{\text{s}}$. As can be seen from the figure, the lobes clearly progress outwards from the outflow's center as a function of increasing outflow velocity. This suggests that the line-of-sight velocity of the gas in the outflow increases with distance from the outflow's center.

It can also be seen from Figures 1, 2 and 3 that the blue (see Figs. 1a–1e) and red (see Figs. 2e–3e) lobes of the outflow do not overlap on the sky. In fact, there is a gap between the two outflow lobes (roughly between $\alpha_{1950} = 6^{\text{h}}38^{\text{m}}30^{\text{s}}$ and $\alpha_{1950} = 6^{\text{h}}38^{\text{m}}26^{\text{s}}$). While it is possible that this gap is actually the result of a lack of outflowing gas between the two observed outflow lobes, it is more likely that outflowing material situated in the gap is moving at such low velocities that its emission is hidden by that from gas in the surrounding cloud.

It is also clear from the integrated intensity maps that higher velocity emission is confined to a more narrow region than lower velocity emission. In order to illustrate this, a graph of lobe width versus velocity is present in Figure 8. Lobe widths in this graph were calculated by taking the difference between the farthest extents of north and south (measured at the $1.0 \pm 0.4 \text{ K km s}^{-1}$ level) of the lobes for each velocity interval in Figures 1 through 3. As can be seen, the width of the outflow lobes decreases with increasing velocity from the line center. This effect is also seen if one measures the widths of the lobes using other contour levels or half-power contours. This suggests that gas moving at higher velocities is situated interior to gas moving at lower velocities in outflow G.

The morphology of outflow G is also clumpy. For example, two separate enhancements in the integrated intensity of blue CO wing emission can be seen in each of Figures 1a through 1d, and two separate enhancements can also be seen in some of

the maps of red wing emission in Figure 3. Since the ^{12}CO temperatures in the wings of outflow G are very low ($< 3 \text{ K}$), it is likely that the ^{12}CO emission is optically thin and that these enhancements in integrated intensity represent actual enhancements in column density of the outflowing gas. This suggests that the gas itself is actually clumpy.

Inspection of the position-velocity maps in Figures 5 and 6 also shows that outflow G has a “sharp edge” beyond which no high-velocity molecular material is found. For example, in the red wing emission shown in Figure 5 it is clear that east of the $\alpha_{1950} = 6^{\text{h}}38^{\text{m}}46^{\text{s}}$ there is no high-velocity molecular gas. The discontinuity in the velocity of gas at the end of the red lobe suggests the presence of a shock.

Finally, inspection of Figure 2d shows that relatively low-velocity red outflow material is situated on the west side of the outflow, the side where primarily blue wing emission is found. The position-velocity maps in Figures 5 and 6 also show this morphology, with low-velocity red wing emission clearly situated at positions where blue outflow emission is strong.

b) Emission from Dense Gas

Presented in Figure 4 is a map of the integrated intensity of emission from the $J = 2-1$ transition of CS in outflow G. Two morphological features in the map are of interest. There is a strong gradient from east to west in the map, and there is a peak in the CS emission at $\alpha_{1950} = 6^{\text{h}}38^{\text{m}}23^{\text{s}}.7$, $\delta_{1950} = 9^{\circ}58'54''$. The strong gradient is most likely due to the fact that outflow G is at an edge of the Monoceros OB1 molecular cloud. The morphology of emission from CO in the region suggests that this is true as well; to the east of the outflow peak $J = 1-0$ CO temperatures drop below 2 K, while to the west they quickly rise to 6 K and greater. While the gradient in the

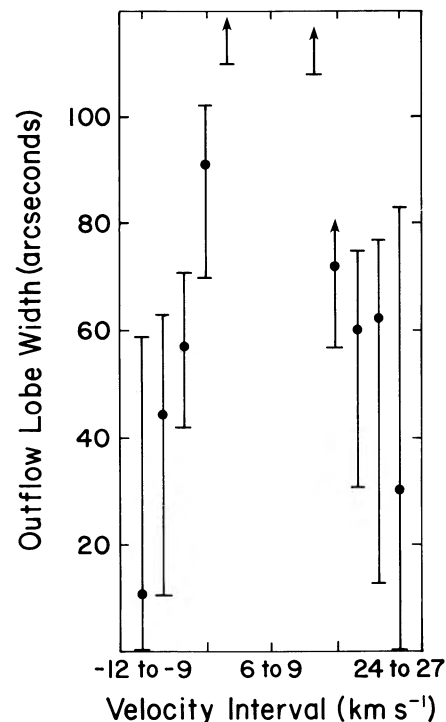


FIG. 8.—Graph showing the variation of the widths of the outflow lobes as a function of velocity. Note that lobe width decreases with increasing velocity from ambient ($\approx 5 \text{ km s}^{-1}$).

TABLE 1
NEAR-INFRARED POINT SOURCES

Source (1)	α_{1950} (2)	δ_{1950} (3)	J mag (4)	H mag (5)	K mag (6)	L' mag (7)	$H-K$ mag (8)	A_v mag (9)
IRS 1.....	6 ^h 38 ^m 24 ^s	9°59'08"	...	10.96 ± 0.05	10.41 ± 0.01	...	0.55 ± 0.05	1.1–5.6
IRS 2.....	6 38 26	9 57 27	...	13.82 ± 0.07	13.61 ± 0.19	...	0.21 ± 0.20	0–3.7
IRS 3.....	6 38 29	9 58 03	12.16 ± 0.01	11.46 ± 0.02	11.23 ± 0.01	...	0.23 ± 0.02	0–2.1
IRS 4.....	6 38 28	9 58 45	...	11.11 ± 0.01	10.99 ± 0.02	...	0.12 ± 0.02	0–1.0
IRS 5.....	6 38 31	9 58 19	15.31 ± 0.11	13.20 ± 0.11	12.35 ± 0.04	...	0.85 ± 0.12	3.4–9.3
IRS 6.....	6 38 33	9 59 32	10.34 ± 0.01	8.93 ± 0.01	8.33 ± 0.01	7.97 ± 0.03	0.60 ± 0.01	2.0–5.7

intensity of CS emission is not surprising, it does make any morphological features associated with outflow G more difficult to identify and interpret. The peak in the CS emission may be associated with outflow G. It is situated between the peaks of the blue and red lobes of the outflow and lies on the line which can be drawn between the peaks of the two lobes. However, it does not lie in the middle of the gap between the two outflow lobes. In the past a number of authors have found CS peaks situated between the red and blue lobes of outflows (see, for example, Rodríguez 1987 and Kaifu 1987 and references therein). These regions of enhanced CS emission have often been interpreted as coming from dense disks associated with star formation. It is possible that these disks play a role in outflow collimation. Whether or not the enhanced CS emission observed arises from a collimating disk is unclear. However, the presence of CS emission does suggest that dense ($n_{\text{H}_2} > 10^4 \text{ cm}^{-3}$) molecular gas exists in the region, and that if any young stellar object associated with outflow G is embedded in that gas it has not yet completely dispersed the dense envelope surrounding it. Further evidence of dense gas in the region has also been reported by Rodríguez and Curiel (1989), who have detected ammonia emission at the position of the CS peak reported here.

c) Infrared Continuum Emission

Molecular outflows are thought to be generated by embedded young stellar objects. In the original *IRAS* survey for such a driving source presented in Margulis and Lada (1986), however, no such source was identified in the direction of outflow G. This was surprising in view of the outflow's extreme velocities and striking morphology. Since such a driving source is likely to exist and since the survey made by Margulis and Lada was biased toward sources bright at 25 μm , we have taken a closer look at the co-added *IRAS* maps of the region and have also made searches in the near-infrared for sources possibly associated with the flow. Altogether searches have now been made at H , K , L' , 12, 25, 60, and 100 μm . Down to our *IRAS* detection limits we find no source possibly associated with outflow G at 12, 25, or 100 μm , respectively. However, there is a 60 μm source with a flux of 3.2 Jy and six near-infrared sources identified at H and K which might possibly be associated with outflow G. Since a far-infrared identification was only made in one *IRAS* band, and since there is a considerable amount of extended emission at 60 μm in the vicinity of outflow G, we feel that the flux at 60 μm should be considered with some skepticism. As a result we treat it as an upper limit in the analysis which follows. On the other hand, the six near-infrared sources all have clear identifications in a number of bands. A list of these point sources along with their positions, J , H , K , and L' magnitudes, and $H-K$ colors is

presented in columns (1) through (8) of Table 1. The visual extinction to these sources, calculated using the intrinsic colors of dwarfs and giant stars in Lee (1970) and Frogel *et al.* (1978) and by using the equation $A_v \approx 10 \times E_{H-K}$, are also listed in column (9). In addition, near-infrared spectral energy distributions for the sources are presented in Figure 9, and the positions of the sources are denoted in Figure 3e (except for IRS 2) and Figure 4. As can be seen IRS 1 lies at the peak of the distribution of CS emission (Fig. 4), and the extinctions to the sources lie between 0 and 10 magnitudes, with the extinction to IRS 5 being greatest. IRS 5 has the most steeply rising near-infrared energy distribution of the sources.

In order to determine whether the near-infrared objects identified are foreground stars, background giants, or young stellar objects embedded in the Mon OB1 cloud, it is worthwhile to compare the extinctions to these objects with that of the Mon OB1 cloud in the region. The visual extinction of the cloud can be derived from the CO and ^{13}CO observations taken at NRO. Line profiles of $J = 1-0$ emission from ^{12}CO

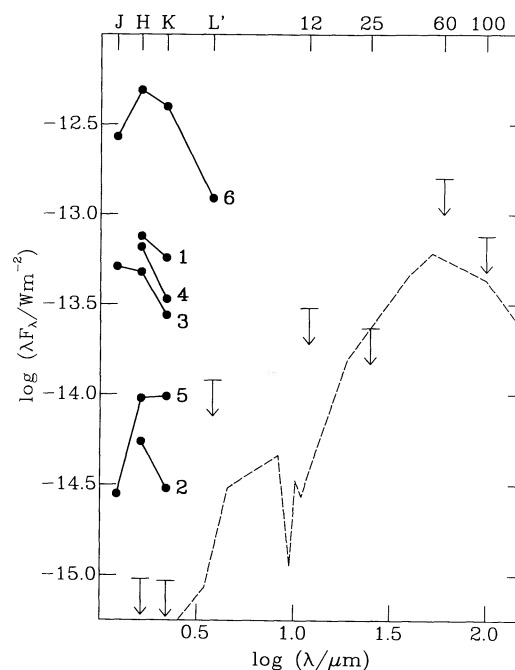


FIG. 9.—Spectral energy distributions (solid lines) of six near-infrared point sources identified in the direction of outflow G. Detection limits of surveys at H , K , L' , 12 μm , 25 μm , 60 μm , and 100 μm are shown. Also shown is the spectral energy distribution (dashed line) of the brightest possible L1551 IRS 5-like source which could exist in the region. Fluxes for L1551 IRS 5 were taken from Cohen and Schwartz (1983) and Cohen *et al.* (1984).

and ^{13}CO at a typical position toward outflow G are shown in Figure 10. Using the ratio of the strengths of these lines (about 4.1) and the width of the ^{13}CO line (about 3.8 km s^{-1}), and assuming an excitation temperature of CO in the ambient cloud of 10 K, the column density of molecular hydrogen in the ambient cloud in the direction of outflow G is $2.8 \times 10^{21} \text{ cm}^{-2}$ (derived using well-known formulae presented, for example, in Margulis and Lada 1985), and the resulting visual extinction is 1.1 magnitudes (derived using $N(\text{H}) = 5 \times 10^{21} \text{ cm}^{-2} \text{ mag}^{-1} A_v$). This extinction is about the same as or less than that toward IRS 1, IRS 2, IRS 5, and IRS 6, and about the same as or greater than that toward IRS 3 and IRS 4. These facts, in combination with the relatively small amount of extinction which could come from the more diffuse interstellar medium in front of and behind the Mon OB1 cloud (in general, $A_v \approx 0.8 \text{ mag per kpc}$, Allen 1973), suggest that IRS 3 and IRS 4 are either embedded in the cloud or are foreground stars, and that IRS 1, IRS 2, IRS 5, and IRS 6 are either background red giants or young stellar objects embedded in the cloud. It would be useful to determine the spectral types of these objects in order to discern between these possibilities (cf. Elias 1978).

If it does turn out that the six sources are embedded in the Mon OB1 cloud, then any one of them could conceivably be associated with outflow G. Each is within about an arcminute ($\approx 0.23 \text{ pc}$, assuming a distance to the flow of 800 pc; Walker 1956) of the center of the outflow, roughly the distance that a central source might be expected to drift (at about a speed of 3 km s^{-1}) during an outflow lifetime (about 10^5 yr). However, the sources most likely to be associated with outflow G are IRS 1 and IRS 5. IRS 1 is a good candidate for the driving source of the outflow since the visual extinction to it is relatively high and since it is coincident with the peak of the CS emission shown in Figure 4. The driving sources of outflows have often been found to be associated with dense cores of gas in molecular clouds (see, for example, Rodríguez 1987 and Kaifu 1987

and references therein). IRS 1 is also coincident with a compact radio continuum source (Rodríguez and Curiel 1989), suggesting that it is surrounded by an H II region and is, in fact, embedded in the molecular cloud. Nevertheless, IRS 5 is also a good candidate since of the six sources the extinction to IRS 5 is highest (and thus IRS 5 is likely to have the most circumstellar material), IRS 5 is the only source with a steeply rising energy distribution in the near-infrared (see Fig. 9), and IRS 5 is the only source which has a spectral energy distribution which can continue to rise in the far-infrared and yet still be below the *IRAS* detection limits. Studies have found that molecular outflows tend to be associated primarily with infrared sources which have flat or rising energy distributions in the far-infrared (Lada 1987). We conclude, therefore, that although it is difficult to tell which near-infrared source, if any, is associated with outflow G, IRS 1 and IRS 5 are the most likely candidates. Using the measured magnitudes at *H* and *K* and the *L'* and *IRAS* limits of detection, the luminosity from $2 \mu\text{m}$ to $100 \mu\text{m}$ of IRS 1 could be as high as $4.5 L_\odot$. Using the measured magnitudes at *J*, *H*, and *K*, and the *L'* and *IRAS* limits of detection, the luminosity of IRS 5 could be as high as $3.6 L_\odot$.

Of the six $2 \mu\text{m}$ sources, IRS 6 has significantly brighter fluxes and probably a significantly higher luminosity than the others. Using the measured magnitudes of this source at *J*, *H*, *K*, and *L'*, and the *IRAS* limits of detection, we estimate that if this source is embedded in the Mon OB1 cloud, its luminosity from $1 \mu\text{m}$ to $100 \mu\text{m}$ could be as high as $14.7 L_\odot$. However, we feel that it is unlikely that IRS 6 is the driving source of outflow G. It has a falling spectral energy distribution between $2 \mu\text{m}$ and $4 \mu\text{m}$ and is not situated coincident with the peak of CS emission shown in Figure 4.

If none of the near-infrared sources turns out to be associated with the outflow, then the luminosity from 2 to $100 \mu\text{m}$ of an associated source (using limits at *K*, *L'*, and the *IRAS* bands) could be as high as $3.5 L_\odot$. Furthermore, if such a source has a spectral energy distribution like that of L1551 IRS 5, the source associated with the well-known outflow in L1551, then its bolometric luminosity would be even lower, not more than about $1.9 L_\odot$.

d) Molecular Hydrogen Emission

Emission from the $v = 1-0 S(1)$ transition of molecular hydrogen was detected at the position $\alpha_{1950} = 6^{\text{h}}38^{\text{m}}19^{\text{s}}.6$, $\delta_{1950} = 9^{\circ}58'47''.5$. This position is marked in Figures 3e and 4. This emission was unresolved in the $19''.6$ aperture used for the observations. The molecular hydrogen emission is situated on the sky within the blue lobe of the outflow. In order to determine the excitation properties of this emission, a spectrum showing the *S* and *Q* branches of emission from the molecule was taken at the position. This spectrum is shown in Figure 11. As discussed in many other studies of molecular hydrogen emission (for example, Shull and Beckwith 1982; Hayashi *et al.* 1985; Lane and Bally 1986) the observed ratio (about 5 to 7) of the heights of the $v = 1-0 S(1)$ and $v = 2-1 S(1)$ lines shown in the spectrum suggests that the molecular hydrogen at this position has been excited into emission by its passage through a shock. This in turn suggests that the molecular hydrogen emission is, in fact, physically associated with the outflow. Shock-excited line emission from molecular hydrogen typically occurs in gas with a temperature of $1-3 \times 10^3 \text{ K}$ (Fischer, Righini-Cohen, and Simon 1980; Shull and Beckwith 1982; Beckwith *et al.* 1983). A value for the total luminosity emitted due to all

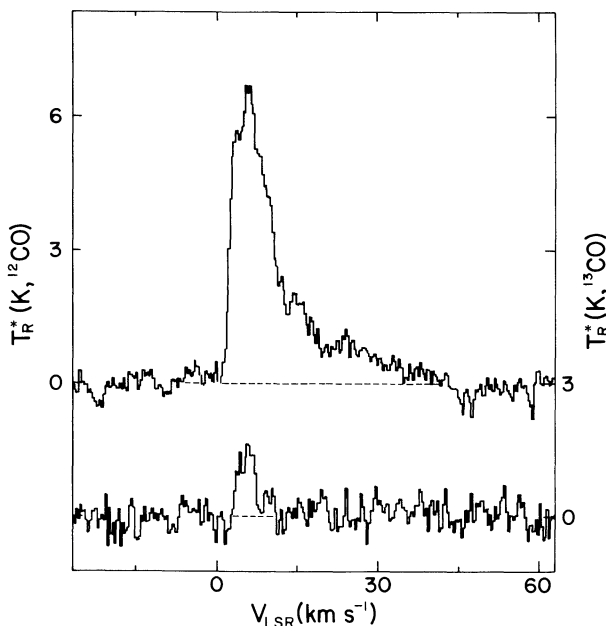


FIG. 10.—Spectra of ^{12}CO and ^{13}CO emission taken with the NRO telescope toward a typical position ($\alpha_{1950} = 6^{\text{h}}38^{\text{m}}39^{\text{s}}$, $\delta_{1950} = 9^{\circ}58'28''$) in the direction of outflow G.

H_2 cooling lines can be estimated from the flux emitted in the $\nu = 1-0$ $S(1)$ line shown in the figure. This value is given by

$$L_{\text{Total}} = 10 \times 4\pi d^2 F_{S(1)} \times 10^{A_{2.2}/2.5},$$

where d is the distance to the source of H_2 emission, $F_{S(1)}$ is the flux in the $\nu = 1-0$ $S(1)$ line, and $A_{2.2}$ is the extinction at $2.2 \mu\text{m}$ to the emitting gas (cf. Lane and Bally 1986). The first factor of 10 in the equation is the theoretically derived ratio of the total intensity from H_2 in all lines to the intensity of H_2 in the $\nu = 1-0$ $S(1)$ line alone for gas at a temperature of 2000 K (cf. Scoville *et al.* 1982). The total luminosity, then, can be calculated using a distance to outflow G of 800 pc (Walker 1956), a flux in the $\nu = 1-0$ $S(1)$ line of $2.5 \times 10^{-20} \text{ W cm}^{-2}$ as measured from Figure 11, and an upper limit to the $2.2 \mu\text{m}$ extinction to the outflow of 0.11 magnitudes (derived from the visual extinction presented above and using $A_{2.2} \approx 0.1 \times A_v$). These numbers yield a total luminosity emitted by H_2 of 0.05 ($10^{A_{2.2}/2.5}$) L_\odot or 0.06 L_\odot .

IV. DISCUSSION

The morphology of CO emission from outflow G suggests that (1) the line-of-sight velocity of molecular material in outflow G increases with increasing distance from the outflow's center, (2) molecular material moving at the highest velocities in outflow G is surrounded by material moving at lower velocities, (3) the structure of outflow G is clumpy, and (4) the outflow possesses a sharp edge beyond which no high-velocity emission is seen. These physical properties suggest at least two possible geometrical models for the outflow. If, for example, the density distribution of the material in the parent molecular cloud which was then swept up by the outflow was relatively smooth, then the increasing velocity of the outflow with distance from its center suggests that at least some material in the outflow is being continuously accelerated along its entire length. In this case the fact that the highest velocity material is situated interior to the lowest velocity material suggests that the low-velocity gas is situated in a shell which surrounds a cavity in which higher velocity material is being accelerated. The density of gas interior to the low-velocity shell is likely to

be lower than that in the shell; otherwise it is difficult to see how material could appear to be accelerated all along the outflow lobes. On the other hand, it is also possible (and perhaps more likely) that material in the parent cloud has a highly inhomogeneous density distribution. In this case the agent which drives the molecular outflow might be expected to quickly accelerate the lowest mass clumps of material to very high velocities while leaving the highest mass clumps moving slowly. These clumps, by virtue of their differing velocities, would then sort themselves out along the outflow lobes with the low-mass, high-velocity clumps ultimately moving to the ends of the lobes, and the high-mass, low-velocity clumps remaining nearer the outflow's center. In this case the fact that lower velocity material surrounds higher velocity material in the outflow still suggests the presence of a low-velocity shell, but the observed increasing velocity of outflow material with distance from the outflow's center could be explained without a continuous acceleration of material all along the outflow lobes. It is difficult to discern between these two models of the origin of the velocity distribution of the CO observed in outflow G. However, the fact that the morphology of the observed outflowing gas is clumpy, along with the growing realization that giant molecular clouds are in general clumpy (see, for example, Matsakis *et al.* 1981; Blitz 1987; Taylor and Dickman 1989), lends credence to the latter possibility.

There are now a number of cases in which observations suggest that outflows consist of a low-velocity molecular shell surrounding a cavity occupied by higher velocity material (cases in addition to outflow G: L1551, Snell, Loren, and Plambeck 1980; Snell and Schloerb 1985; Uchida *et al.* 1987; Moriarty-Schieven *et al.* 1987; Moriarty-Schieven and Snell 1988; NGC 2071, Fukui *et al.* 1987; Moriarty-Schieven, Snell, and Hughes 1989; GL 490, Fukui *et al.* 1987; IRAS 1629a, Walker *et al.* 1988; and Mon R2, Wolf, Lada, and Bally 1989; B335, Moriarty-Schieven and Snell 1989). That this structure has been observed now in a number of cases suggests that it may be common to outflows in general.

We have also found low-velocity red wing emission partly mixed on the sky with the blue lobe of outflow G. Red wing emission in the blue lobe and vice versa has been observed in the past in a number of other outflows as well (examples in addition to outflow G: L1551, Uchida *et al.* 1987; Moriarty-Schieven *et al.* 1987; Moriarty-Schieven and Snell 1988; RNO 43 and B335, Cabrit, Goldsmith, and Snell 1988; NGC 2071, Moriarty-Schieven, Snell, and Hughes 1989; Moriarty-Schieven and Snell 1989). However, there is considerable controversy over the meaning of this aspect of flow morphology. It has been interpreted as evidence that outflow lobes are in rotation about their long axes (Uchida *et al.* 1987), that molecular material is being ablated off dense molecular clumps in outflows (Moriarty-Schieven *et al.* 1987), and that the opening angles of the outflows are large enough (for a given inclination) to permit detection of both red and blue emission from the near and far sides of a given outflow lobe (Cabrit, Goldsmith, and Snell 1988; Rice and Lada 1989). Unfortunately, at present we are unable to distinguish between these possibilities for outflow G.

Finally, outflow G is also bipolar and very highly collimated, and its energetics are striking as well. This outflow is 4 times longer than it is wide on the sky (see Figs. 1-3), making it one of the most highly collimated outflows yet identified. Furthermore, the ratio of the luminosity of any young stellar object associated with it to its mechanical luminosity is very

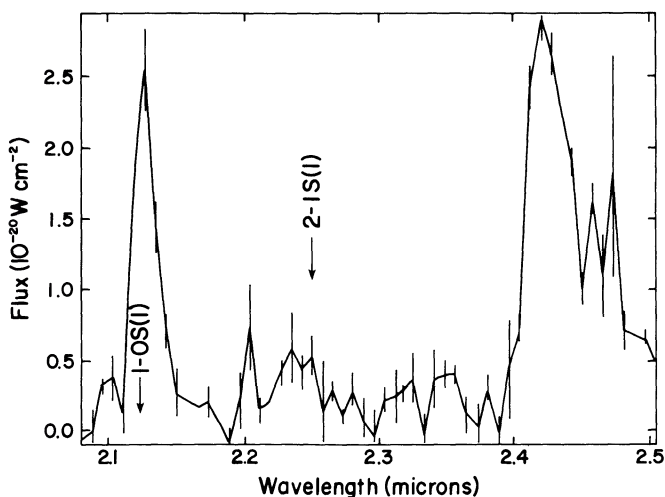


FIG. 11.—Spectrum of $2 \mu\text{m}$ H_2 emission taken at the position $\alpha_{1950} = 6^{\text{h}}38^{\text{m}}19^{\text{s}}.6$, $\delta_{1950} = 9^{\circ}58'47''.5$. The wavelengths at which the $\nu = 1-0$ $S(1)$ and $\nu = 2-1$ $S(1)$ lines occur are marked. The many vertical lines in the figure represent the 1σ errors in the fluxes at each wavelength.

low, much lower than for other outflows now known. The luminosity of any young stellar object physically associated with outflow G must be less than about $4.5 L_{\odot}$. In comparison, the mechanical luminosity carried by outflow G must be at least $1.9 L_{\odot}$ (Margulis, Lada, and Snell 1988), in fact, at least $2.5 L_{\odot}$ if one includes in the mass of the outflow the contribution of helium associated with the molecular gas. This suggests that the ratio of the luminosity of the driving source of outflow G to its mechanical luminosity is no greater than 1.8, a value much lower than that found for other outflows (50–500, Lada 1985).

The low ratio of driving source to wind luminosities for outflow G suggests that it is impossible for this outflow to be driven by radiation pressure from a central source since conversion efficiencies of at least 56% from stellar to wind luminosity would be required. Furthermore, the low ratio of luminosities, as well as the highly collimated appearance of outflow G, may be indications of the effects of the structure of a surrounding cloud on the ability of an outflow to form. Outflow G is situated in what is likely to be a relatively low density region near the edge of the Monoceros OB1 molecular cloud (peak temperatures of line emission from the $J = 1-0$ transition of CO in the direction of the outflow are only a few degrees—see Figure 10 in this paper or Figure 6 in Margulis, Lada, and Snell 1988). As a result, it is possible that a low average density of material in this portion of the cloud may have allowed the outflow to expand nearly unimpeded into the molecular cloud around it, thus allowing the bipolar flow to become very extended and achieve relatively high outflow velocities. Evidence that the density of the ambient cloud must play some role in the formation of the outflow can be seen in Figures 5 and 6 in which the redshifted outflow lobe, which is expanding away from the core of the cloud, appears to extend to higher velocities than the blueshifted lobe, which is expanding into the cloud.

V. CONCLUSIONS

We have made detailed observations of CO, CS, infrared continuum, and H_2 emission from the outflow NGC 2264G in the Monoceros OB1 Molecular cloud. From the high-resolution observations of CO emission, we find that the outflow is bipolar and highly collimated. It appears that

molecular material in each lobe of the outflow is situated in a shell with material moving at higher velocities situated interior to material moving at lower velocities. The velocities at which molecular material is observed also appear to increase with increasing distance from the outflow's center. Furthermore, the distribution of CO in the lobes of the outflow appears to be clumpy. The highly collimated appearance of the outflow may be due to the fact that it has formed in a low-density portion of the Monoceros OB1 molecular cloud.

Molecular hydrogen emission has been detected in the direction of the blueshifted lobe of the outflow. The total luminosity emitted by molecular hydrogen in the outflow is estimated to be $0.05 (10^{A_{2.2}/2.5}) L_{\odot}$.

A small peak in an otherwise steeply decreasing distribution of CS emission is found between the peaks of the red and blue lobes of the outflow. This peak may indicate the presence of a small dense core in which the driving source of the flow may be located.

Six $2 \mu\text{m}$ sources have been identified in the direction of the outflow. Of these two are more likely than the others to be physically associated with the flow. The extinction to IRS 1 is relatively high and it is coincident with the peak of the CS emission. IRS 5 is the only source of the six which has a spectral energy distribution which is steeply rising to the far-infrared. Any source physically associated with the outflow must have a bolometric luminosity less than about $4.5 L_{\odot}$.

The low luminosity of the driving source of the outflow suggests that it is impossible for this flow to be driven through stellar radiation from a central source since conversion efficiencies in excess of 50% from stellar luminosity to flow mechanical luminosity would be required. Furthermore, the high ratio of wind mechanical luminosity to stellar luminosity for this flow is higher than observed toward any known outflow and may be a consequence of the fact that the flow has formed in a relatively low density portion of the Monoceros OB1 molecular cloud.

We thank Steve Strom, John Kwan, and Ron Snell for useful discussions and helpful criticism. This research was supported in part by National Science Foundation grants AST 88-15406 and AST 88-15753 and IRAS Guest Investigator grant NAS7-918.

REFERENCES

- Allen, C. W. 1973, *Astrophysical Quantities* (London: Althone).
 Beckwith, S., Evans, N. J., II, Gatley, I., Gull, G., and Russell, R. W. 1983, *Ap. J.*, **264**, 152.
 Blitz, L. 1987, in *Physical Processes in Interstellar Clouds*, ed. G. E. Morfill and M. Scholer (Dordrecht: Reidel), p. 35.
 Cabrit, S., Goldsmith, P. F., and Snell, R. L. 1988, *Ap. J.*, **334**, 196.
 Cohen, M., and Schwartz, R. D. 1983, *Ap. J.*, **265**, 877.
 Cohen, M., Harvey, P., Schwartz, R. D., and Wilking, B. A. 1984, *Ap. J.*, **278**, 671.
 Elias, J. H. 1978, *Ap. J.*, **224**, 453.
 Fischer, J., Righini-Cohen, G., and Simon, M. 1980, *Ap. J. (Letters)*, **238**, L155.
 Frogel, J. A., Persson, S. E., Aaronson, M., and Matthews, K. 1978, *Ap. J.*, **220**, 75.
 Fukui, Y., Iwata, T., and Takano, T. 1987, in *Star Forming Regions*, ed. M. Peimbert and J. Jugaku (Dordrecht: Reidel), p. 328.
 Hayashi, M., Hasegawa, T., Gatley, I., Garden, R., and Kaifu, N. 1985, *M.N.R.A.S.*, **215**, 31P.
 Kaifu, N. 1987, in *Star Forming Regions*, ed. M. Peimbert and J. Jugaku (Dordrecht: Reidel), p. 275.
 Kutner, M. L., and Ulich, B. L. 1981, *Ap. J.*, **250**, 341.
 Lada, C. J. 1985, *Ann. Rev. Astr. Ap.*, **23**, 267.
 ———. 1987, in *Star Forming Regions*, ed. M. Peimbert and J. Jugaku (Dordrecht: Reidel), p. 1.
 Lada, C. J., Margulis, M., Sofue, Y., Nakai, N., and Handa, T. 1988, *Ap. J.*, **328**, 143.
 Lane, A. P., and Bally, J. 1986, *Ap. J.*, **310**, 820.
 Lee, T. A. 1970, *Ap. J.*, **162**, 217.
 Margulis, M., and Lada, C. J. 1985, *Ap. J.*, **299**, 925.
 ———. 1986, *Ap. J. (Letters)*, **309**, L87.
 Margulis, M., Lada, C. J., and Snell, R. L. 1988, *Ap. J.*, **233**, 316.
 Margulis, M., Lada, C. J., and Young, E. T. 1989, *Ap. J.*, **345**, 906.
 Matsakis, D. N., Hjalmarsen, A., Palmer, P., Cheung, A. C., and Townes, C. H. 1981, *Ap. J. (Letters)*, **250**, L85.
 Moriarty-Schieven, G. H., and Snell, R. L. 1988, *Ap. J.*, **332**, 364.
 ———. 1989, *Ap. J.*, **338**, 952.
 Moriarty-Schieven, G. H., Snell, R. L., and Hughes, V. A. 1989, *Ap. J.*, **347**, 358.
 Moriarty-Schieven, G. H., Snell, R. L., Strom, S. E., Schloerb, F. P., Strom, K. M., and Grasdalen, G. L. 1987, *Ap. J.*, **319**, 742.
 Rice, B., and Lada, C. J. 1989, in preparation.
 Rodriguez, L. F. 1987, in *Star Forming Regions*, ed. M. Peimbert and J. Jugaku (Dordrecht: Reidel), p. 239.
 Rodriguez, L. F., and Curiel, S. 1989, preprint.
 Scoville, N. Z., Hall, D. N. B., Kleinmann, S. G., and Ridgeway, S. T. 1982, *Ap. J.*, **253**, 136.
 Shull, J. M., and Beckwith, S. 1982, *Ann. Rev. Astr. Ap.*, **20**, 163.
 Snell, R. L., Loren, R. B., and Plambeck, R. L. 1980, *Ap. J. (Letters)*, **239**, L17.

- Snell, R. L. 1981, *Ap. J. Suppl.*, **45**, 121.
Snell, R. L., and Schloerb, F. P. 1985, *Ap. J.*, **295**, 490.
Taylor, D. K., and Dickman, R. L. 1989, *Ap. J.*, **341**, 293.
Uchida, Y., Kaifu, N., Shibata, K., Hayashi, S. S., and Hasegawa, T. 1987, in *Star Forming Regions*, ed. M. Peimbert and J. Jugaku (Dordrecht: Reidel), p. 287.
- Ulich, B. L., and Haas, R. W. 1976, *Ap. J. Suppl.*, **30**, 247.
Walker, C. K., Lada, C. J., Young, E. T., and Margulis, M. 1988, *Ap. J.*, **332**, 335.
Walker, M. F. 1956, *Ap. J. Suppl.*, **2**, 365.
Wolf, G., Lada, C. J., and Bally, J. 1989, in preparation.

I. GATLEY: National Optical Astronomy Observatories, P.O. Box 26732, Tucson, AZ 85726-6732

T. HASEGAWA, M. HAYASHI, and N. KAIFU: Nobeyama Radio Observatory, Tokyo Astronomical Observatory, Nobeyama, Minamisaku, Nagano, 384-13, Japan

S. S. HAYASHI: Joint Astronomy Center, Hawaii Headquarters, 665 Komohana Street, Hilo, HI 96720

T. P. GREENE, C. J. LADA, and E. T. YOUNG: Steward Observatory, University of Arizona, Tucson, AZ 85721

M. MARGULIS: Five College Radio Astronomy Observatory, University of Massachusetts, Amherst, MA 01003